7668 *Macromolecules* **2010**, *43*, 7668–7679
DOI: 10.1021/ma1014403

Macromolecules
ARTICLE

Morphology, Phase Composition, and Molecular Mobility in Polyamide Films in Relation to Oxygen Permeability

V. M. Litvinov,*,† O. Persyn,‡ V. Miri,‡ and J. M. Lefebvre‡

†*DSM Resolve, P.O. Box 18, 6160 MD Geleen, The Netherlands, and* ‡*Université de Lille Nord de France, Centre National de la Recherche Scientifique, Université de Lille 1, Unité Matériaux et Transformations, Batiment C6, Cité Scientifique, 59655 Villeneuve d' Ascq, France*

Received June 30, 2010; Revised Manuscript Received August 3, 2010

ABSTRACT: The effect of phase composition and molecular mobility on oxygen permeability is studied for stretched films prepared from polyamide 6 (PA6) and a blend of PA6 with semiaromatic amorphous polyamide (aPA)−PA6/aPa, which is a random co-polyamide containing iso- and terephthalic chain units. The effect of stretching degree of films on crystallinity and strain-induced immobilization of the amorphous phase is studied by DSC and solid-state proton NMR transverse (T_2) magnetization relaxation, respectively. Changes of these parameters upon strain are determined. Crystallinity and T_g are hardly affected by strain, as shown by DSC. Molecular mobility in the amorphous phase of stretched films is largely restricted upon increasing strain. At temperatures well above T_g, the amorphous phase consists of two fractions of nanometer thickness: one behaves like glassy polyamides, and the other one, a semirigid fraction, reveals largely hindered chain mobility. The amount of the glassy-like fraction increases proportionally to the strain. In addition, molecular mobility in the semirigid fraction decreases with increasing strain. According to high-resolution solid-state ^{13}C NMR experiments, the composition of the semirigid fraction in PA6/aPA films is enhanced by aPA. It is shown that the immobilization of the amorphous phase has a large influence on the permeability of the films. It appears that oxygen permeability correlates well with a parameter describing strain-induced decrease in molecular mobility in the amorphous phase. This parameter is the reciprocal product of the amount of the semirigid fraction at temperatures well above T_g and molecular mobility in this fraction as determined by NMR T_2 relaxation time. It is suggested that the semirigid fraction of the amorphous phase could be considered as "channels" for diffusion of oxygen molecules. Despite lower oxygen solubility in PA6 films, as shown by low-temperature proton NMR T_1 relaxation data, the permeability of all PA6/aPA films under humid conditions is significantly lower than that of PA6 films. It is suggested that the lower permeability of PA6/aPA films is due to complex formation between oxygen molecules and aromatic rings of aPA, which slows down oxygen diffusion. Results of the present study are of interest for a better understanding of both permeability of polyamide films and other phenomena in polyamides that are affected by transport properties of small molecules, such as the rate of water uptake, dyeability of fibers, thermal oxidation, and blooming.

I. Introduction

High thermal stability as well as good mechanical and barrier properties of polyamides determine a wide application area of these polymers for food packaging. Processing conditions that are used for preparation of polyamide films largely influence morphology, physical, and transport properties. Therefore, knowledge of processing−morphology−permeability relationships is of a large importance for improvement of barrier properties of polyamide films.

The permeation of gas or vapor molecules through a polymer film involves the following stages: (1) absorption of penetrant molecules on to the film surface; (2) solution of the penetrant molecules in the film; (3) diffusion through the film; and (4) desorption from the other surface of the film. Solubility (S) and diffusivity (D) are the intrinsic characteristics determining transport or barrier properties of penetrant molecules in a host material. Both characteristics are governed by specific interactions, molecular mobility, size and shape of penetrant molecules, and morphology in the case of heterogeneous polymers. The permeability (P) is the product ($P = SD$) of solubility, which is a thermodynamic parameter, and diffusivity, which is a kinetic parameter. The permeability is usually used for describing the transport rate at steady state.

The sorption and transport properties of small molecules are largely influenced by several physical structures and morphology of semicrystalline polymers.[1] The following characteristics should be discussed in this respect. Degree of crystallinity is one of the most important parameters since crystalline regions are generally inaccessible to the most types of penetrant molecules. Hence, on the one hand, crystalline domains act as excluded volume for sorption of small molecules decreasing solubility, whereas on the other hand, crystallites form impermeable barriers for diffusion process increasing the average path length for penetration of small molecules through a material made from semicrystalline polymers. These two effects can be described by the tortuosity factor: $\tau = 1 + (L/2W)\phi_c$, where L and W are the length and width of crystalline domains and ϕ_c is the volume fraction of crystalline or rigid phase.[2] If permeability is studied for stretched polymer films, crystal orientation can also significantly affect the permeability.[2]

Another characteristic of semicrystalline polymers, which is largely influenced by the degree of crystallinity, is molecular mobility in the amorphous phase which determines the rate of

*To whom correspondence should be addressed. E-mail: victor.litvinov@dsm.com.

 Published on Web 08/13/2010

local density fluctuations. A close relationship between permeability and molecular mobility in the amorphous phase of semicrystalline polymers has been demonstrated.[3,4] The effect of molecular mobility on permeability is obvious from a large difference in the diffusion rate of small molecules in polymer melts as compared to glassy polymers. The diffusion rate decreases by approximately 2−3 orders of magnitude upon vitrification.[5] At temperatures well above T_g, fast local chain motions cause rapid density fluctuations and the diffusion rate of small molecules is largely determined by the rate of these density fluctuations. Contrary to polymer melts, the residence time of penetrant molecules in the accessible volume ("cavities") in glassy polymers is much longer than time between successive jumps between neighboring cavities. Crystallization of polymers causes large immobilization of the amorphous phase since crystallites (1) act as physical network junctions restricting chain mobility in the amorphous phase and (2) form topological barriers increasing the anisotropy of chain motions in the amorphous phase. These restrictions on the chain mobility depend on both crystallinity and the number of crystallites (their dimensions) in the unit volume of semicrystalline polymers. The effect of cross-linking on the permeation is well-known for amorphous rubbers. An increase in cross-link density causes a decrease in the diffusion coefficient and an increase in the activation energy for diffusion and makes the diffusion process more dependent on the size and shape of penetrant molecules.[6−9] Molecular mobility[10] and diffusion coefficient of small molecules in rubbers decrease approximately linearly with cross-link density at low and moderate cross-linking.[11] At higher network densities, the dependence deviates from linear.[11]

Different phenomenological and molecular models have been used for describing the diffusion process and permeability in polymers.[6,12,13] Molecular models would seem to offer a better description of transport properties. However, all such models involve one or more adjustable parameters limiting quantitative analysis of experimental results in the relation to molecular characteristics. In order to understand diffusion of small molecules in semicrystalline polymers, quantitative characterization of morphology, phase composition, and molecular mobility are of great importance. In this respect, the phase structure is probably one of the most important parameters, mainly because the amorphous and crystalline phases exhibit vastly different behavior. Since crystallites are generally inaccessible to most penetrant molecules, characterization of noncrystalline regions is of special interest with respect to transport properties. Traditionally, a two-phase model is used to describe the morphology of semicrystalline polymers. However, this model with constant densities of crystalline and amorphous phases is rather simplified due to the presence of a crystal−amorphous interface[14−19] and/or rigid fraction of the amorphous phase.[20−24] Since properties of the interface or rigid amorphous fraction are intermediate between those of the crystalline and amorphous phases, the presence of the interfacial layer, which is usually counted for noncrystalline fraction, could largely influence the permeability. Therefore, the two-phase model often fails to provide a good description of the permeability and other physical properties of semicrystalline polymers.[25−29] For example, chain mobility in the interfacial layer of polyamide 6 (PA6) fibers is largely hindered and water molecules are hardly absorbed by the interfacial layer.[30] As far as stretched films are concerned, molecular mobility in the amorphous phase is restricted upon drawing PA6 fibers and films.[30,31] However, no quantitative relationship between chain orientation in the amorphous phase and permeability is known for these materials.

Recent atomistic simulations have shown that diffusivity of small molecules in polymers is controlled by the mechanism and the frequency of chain motion.[5,23,33−35] It should be noted that "the permeation is a phenomenon encompassing mechanisms that span a wide spectrum of time and length scales exceeding by many orders of magnitude the corresponding scales that can't be tracked by conventional atomistic molecular dynamics (MD) and Monte Carlo (MC) simulation techniques".[5] Therefore, experimental studies of chain mobility in the relation to permeability are of significant importance for better understanding barrier properties of polymers. Solid-state NMR is one of the most powerful techniques for investigation of morphology and molecular mobility in polymeric materials.[36−39] When the term crystallinity is used in connection with low-resolution NMR technique, this refers to the rigid fraction at temperatures well above T_g, i.e., the fraction of material possessing the lowest molecular mobility, and to distinguish this material from semirigid and soft noncrystalline materials (either oriented or nonoriented).[30]

The phase composition, domain sizes, and molecular mobility in crystalline and amorphous phases of PA6 fibers and melt-crystallized PA6 have been studied by several groups using solid-state NMR techniques. Results of these studies have recently been reviewed.[30] Above the glass transition temperature, various NMR methods have revealed two types of amorphous regions in PA6, i.e., amorphous regions with less constrained chain fragments—soft amorphous fraction—and semirigid crystal−amorphous interface where molecular mobility is lower. These noncrystalline regions significantly differ in *local chain mobility*. It is suggested that information about molecular mobility in the less constrained (more mobile) amorphous fraction and its amount are of particular interest in the relation to diffusivity of small molecules in semicrystalline polymers since diffusivity increases with an increase in molecular mobility in the host matrix.[8] Therefore, if some of the molecular characteristics of semicrystalline polymers are related to transport properties of small molecules, the amount of amorphous phase with less constrained chain fragments as well as the molecular mobility of these fragments could be of larger importance as compared to crystallinity.

The establishing of relationships between the chemical structure of the initial polymer, strain which is used for film preparation, resulting morphology, molecular mobility, and functional properties of polyamide films is the subject of great interest. Two types of stretched films are prepared for the present study, i.e., films made from PA6 and from a blend of PA6 with amorphous aromatic polyamide (aPA) which is a random co-polyamide containing 70% of isophthalic and 30% of terephthalic chain units. Films are stretched at two different temperatures, and strain is varied in a wide range from 0% to 200−300%. The aim of this study is to determine (1) the effect of strain on the phase composition, domain sizes, and molecular mobility, (2) the relative difference in oxygen solubility in PA6 and PA6/aPA films and the effect of absorbed water on oxygen solubility, and (3) the effect of these molecular characteristics of the films on oxygen permeability. A number of techniques are used for characterization of the films: film morphology is analyzed by AFM; glass transition and melting behavior by DSC; orientation of crystallites by X-rays; the chemical composition of more mobile amorphous fraction in PA6/aPA film by high-resolution solid-state ^{13}C NMR experiment; and relative difference in oxygen solubility in films, the phase composition, molecular mobility, and domain sizes by proton low-resolution NMR methods.

II. Experimental Section

A. Materials. This paper is focused on two types of polyamide films that were prepared at DSM (Geleen, The Netherlands): films from polyamide 6 (PA6) and those from a blend of PA6 with an amorphous aromatic polyamide (aPA). The blend was composed of 60 wt % PA6 and 40 wt % aPA. The PA6 had a

weight-average molecular weight M_w = 50 000 g/mol and a specific density d = 1.132 g/cm^3. Amorphous aromatic polyamide (PA6I-6T, grade Grivory G21 from EMS) was a random co-polyamide that was obtained by polycondensation of hexamethylenediamine with terephthalic and isophthalic acids. It contained 70% of isophthalic and 30% of terephthalic chain units. M_w and specific density of aPA were 8120 g/mol and 1.18 g/cm^3, respectively.

B. Film Preparation. The PA6 and PA6/aPA blend were extruded in a single-screw extruder at 275 °C. The materials were cast into films of ~80 μm thick and cooled on a chill roll at 100 °C. Since fast cooling of PA6/aPA film prevents full crystallization of PA6,[40] the film was annealed at 110 °C for 5 min to favor the cold crystallization. In order to work with dry samples, these films were stored under vacuum at room temperature. Uniaxial stretching of the films was conducted on an Instron machine equipped with a temperature-controlled oven. Stretching of the films was performed at two temperatures: 100 and 130 °C, with an initial strain rate of 3.5×10^{-2} s^{-1}. With these conditions, the stretching was stopped when different strain values ε of 50%, 100%, 150%, 200%, and 300% were reached. The strain ε is defined as the ratio $[(L - L_0)/L_0] \times 100\%$, where L_0 and L are the sample gauge length before and after drawing, respectively. The uniaxial "post-mortem" local strain was determined from the displacement of ink marks printed on the sample surface prior to stretching. The marks were initially spaced by 1.5 mm.

C. Characterization of Polyamide Films. *C.1. Oxygen Permeability*. The permeability was determined with a Mocon Oxtran 2/21 oxygen permeameter. Sample surface area was 5 cm^2. All experiments were performed at 23 °C and 85% relative humidity and under atmospheric pressure.

C.2. DSC. The differential scanning calorimetry experiments were carried out on a Perkin-Elmer Diamond device. The heating and cooling rates were 10 °C/min, and the sample weight was ~10 mg. The glass transition temperature T_g was taken at the middle of the heat capacity jump, whereas the melting point T_m and the crystallization temperature T_c were measured at the maximum and the minimum of the enthalpic peaks, respectively. Crystallinity was determined as the ratio of the heat of fusion of the sample (ΔH_m) to the heat of fusion of the crystalline phases of PA6 ($\Delta H_m°$). $\Delta H_m°$ of 230 J/g is often used for the estimation of DSC crystallinity of PA6.[41] However, it should be noted that, in general, different methods for crystallinity determination do not always yield the same results on exactly the same sample, as has been shown previously.[14,30,42]

C.3. Solid-State NMR

C.3.1. Sample Preparation. For low-resolution proton NMR relaxation experiments, ~0.4 g of film was cut into pieces of approximately 2 × 2 mm, and the pieces were packed in an NMR glass tube with a diameter of 9 mm. No specific procedure was followed to ensure a random packing of film pieces in the sample tube. Because of the large size of the NMR tube compared to the dimensions of the pieces, however, it is safe to assume that the pieces do not preferably orientate themselves toward the direction of the magnetic field of the NMR spectrometer. Care was taken in preconditioning of the samples before starting NMR experiments. Polyamides tend to absorb moisture, and the equilibrium moisture content is a function of the relative humidity of the surrounding air. The NMR experiments were performed for dried films. Films were dried in the NMR tube for 20 h at room temperature and a vacuum of about 1 mmHg. After drying, the tube was filled with dried nitrogen. The sample tube was tightly closed with a Teflon cylinder, the bottom part of which was slightly above the upper part of the sample. Two films were also studied after they were saturated with water at 23 °C in a climate room with 85% relative humidity (85% RH).

Low-resolution proton NMR T_1 relaxation experiment for PA6 and PA6/aPA films saturated with water and the films under dry nitrogen and air were performed using a 9 mm NMR tube with a valve on the top of the tube. This experiment was used to determine the relative difference in oxygen solubility in these films. After films were dried as described above, the tube was filled either with dried nitrogen or air. After the T_1 value of the dried films was measured as a function of temperature, the tubes were placed in a climate room at 23 °C with RH of 85% for 1 month.

C.3.2. NMR Equipment. Low-resolution proton NMR T_1 and T_2 relaxation experiments were performed on a Bruker Minispec MQ-20 spectrometer on static samples. This spectrometer operates at a proton resonance frequency of 20 MHz. The length of the 90° pulse and the dead time were 2.8 and 7 μs, respectively. A BVT-2000 temperature controller was used for temperature regulation with an accuracy of ±0.1 °C. The temperature gradient within the sample volume was less than 1 °C. The temperature at the sample position was measured separately using a RTD sensor Pt100 with a diameter of 0.5 mm inserted in the middle of the sample.

High-resolution ^{13}C NMR experiments were carried out at 110 and 130 °C with a Varian Inova 400 MHz spectrometer equipped with a 7 mm variable temperature CPMAS probe. Dry nitrogen was used for spinning of 7 mm NMR rotor under the magic angle. The spinning speed was set to 7 kHz. The rotor cap had a small hole in the center through which absorbed water was removed from the sample before the experiment was started. The 90° pulse length in proton and carbon channels was 5 μs, and the recycle delay was 4 s. The acquisition of the carbon signal was performed under a proton-decoupling field of 50 kHz. Adamantane was used to optimize the Hartmann−Hahn condition, and it also served as an external secondary chemical shift reference (38.3 ppm for the methylene resonance relative to tetramethylsilane).

C.3.3. NMR Experiments and Data Analysis. Partitioning of PA6 and aPA between rigid and semirigid fractions of the amorphous phase in unstretched PA6/aPA film was studied by high-resolution ^{13}C NMR inversion−recovery cross-polarization experiment (IRCP). The cross-polarization time τ_{cp} was 1.5 ms. A variable "inversion" time τ_{in} (during which the phase of the proton spin-look field was shifted by 180°) was varied from 0 to 0.5 ms.

The phase composition and molecular mobility in polyamide films were studied using the following proton low-resolution NMR experiments. Two methods are commonly used for recording the free induction decay (FID) for static samples: (1) the 90° pulse excitation: $90°_x$−dead time−[acquisition of the amplitude of the transverse magnetization $A(t)$ as a function of time t after the 90° pulse]; (2) the solid-echo pulse sequence (SEPS): $90°_x - t_{se} - 90°_y - t_{se}$−[acquisition of the amplitude of the transverse magnetization $A(t)$], where $t = 2t_{se} + t_{90}$ was set to zero and t_{90} is the duration of the 90° pulse. Both methods could cause systematic errors in the analysis of the phase composition in heterogeneous materials.[30,43] The initial part of the FID is not detected after the 90° pulse excitation because of the dead time of the spectrometer receiver. Therefore, knowledge of the shape of the transverse magnetization decay for the rigid phase/fraction is required for accurate deconvolution of the FID into components corresponding to different phases. The shape of the FID for the rigid fraction of polyamide films was determined by the SEPS. Finally, the phase composition and molecular mobility were determined by analysis of the FID that was recorded after the 90° pulse excitation. The FID experiment took 5 min. Sample exposure to 110 and 140 °C during the NMR experiment did not causes significant change in molecular mobility, and the phase composition as was shown previously for PA6 fibers.[30]

The fractions (% T_2^{index}) and the apparent relaxation times (T_2^{index}) of the relaxation components were obtained by performing a least-squares fit of the data using eq 1. FIDs for unstretched films were fitted with the two-component function (first two terms in eq 1) as well as with the three-component

function which was a linear combination of the stretched exponential ($\alpha < 2$) or Gaussian ($\alpha = 2$) function and two exponential functions. FID for stretched films was fitted with the two-component function which was a linear combination of the stretched exponential or Gaussian function and exponential function.

$$A(t) = A(0)^s \exp[-(t/T_2^s)^\alpha] + A(0)^i \exp[-(t/T_2^i)] + A(0)^l \exp[-(t/T_2^l)] \quad (1)$$

The superscripts "*s*", "*i*", and "*l*" stand for short, intermediate, and long decay time of the relaxation components, respectively. These components correspond to the relaxation of rigid, semirigid, and soft fractions of films. The least-squares fit of FIDs that were measured with the SEPS has shown that α was close to 2 for all samples studied. Therefore, this α value was used for the fit of FIDs, as recorded after the 90° pulse excitation. The fraction of the relaxation components, as designated in the text by $\%T_2^{\text{index}} = \{A(0)^{\text{index}}/[A(0)^s + A(0)^i + A(0)^l]\} \times 100\%$, represents the weight fraction of hydrogen atoms in phases/domains in PA6 that reveal distinct differences in molecular mobility. T_2 value allows the relative difference in molecular mobility to be determined; i.e., the longer the T_2 relaxation time, the larger the amplitude of molecular motions, their frequency, or both.

The relative difference in oxygen solubility was determined using the proton longitudinal (T_1) magnetization relaxation experiment. The recovery rate of the longitudinal magnetization (T_1 relaxation rate $= 1/T_1$) was measured using the inversion–recovery pulse sequence with the solid-echo detection of the signal amplitude: $180°_x - t_{\text{inv}} - 90°_x - t_{\text{se}} - 90°_y - t_{\text{se}}$–[acquisition of the amplitude of the echo maximum $A(0)$ as a function of t_{inv}], where t_{se} was 10 μs. Inversion–recovery curves were fitted with the following exponential function:

$$A(t_{\text{inv}}) = A(0)[1 - 2\exp(-t_{\text{inv}}/T_1)] \quad (2)$$

The T_1 experiment at each temperature was performed after fast cooling of samples from room temperature to the temperature of the experiment.

Domain sizes for another series of PA6 films were estimated using spin-diffusion experiments with a proton double-quantum (DQ) filter. The DQ filter selected the nuclear magnetization from the rigid fraction of PA6 films. The pulse sequence and analysis of the spin-diffusion data have been described previously.[44,45] A global fit, which was used for the analysis of FIDs recorded in the spin-diffusion experiment, has been also described in a previous study.[46]

III. Results

A. Oxygen Permeability of Films. Dried PA6 films display oxygen permeabilities significantly lower those of the PA6/aPA blend. This can be attributed to the higher crystal content in PA6 films in comparison with that in PA6/aPA films. The evolution of permeability with water absorption is different between PA6 and PA6/aPA films. Water absorption causes a large increase in the permeability of PA6 due to the decrease in T_g.[47] By contrast, the permeability of PA6/aPA films slightly decreases upon water uptake. This effect is known for aromatic polyamides,[48–50] and it might be attributed to a competition of water molecules with the permeant gas for free volume excess in the polymer matrix, thereby reducing both oxygen solubility and diffusivity.[49–51]

Oxygen permeability of PA6 and PA6/aPA films under humid conditions is compared in Figure 1. The permeability of both types of films decreases with increasing film strain. The decrease is larger for PA6 films. However, the permeability of even highly strained PA6 films is larger than that of

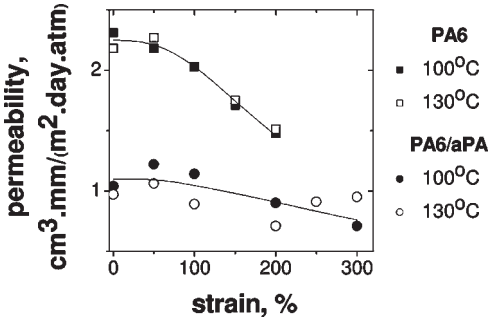

Figure 1. Oxygen permeability of uniaxially stretched PA6 and PA6/aPA films as a function of strain used for film preparation. The permeability was measured at 23 °C and 85% RH. The films were stretched at 100 and 130 °C.

Table 1. Overall Crystallinity, χ_c, Crystallinity of PA6 in Unstretched PA6/aPA films ($\varepsilon = 0\%$), χ_c(PA6), Crystallization, T_c, Melting, T_m, and Glass Transition, T_g, Temperatures of Dried Polyamide Films, As Determined by DSC[a]

film composition PA6–aPA, wt %–wt %	T_g, °C	T_m, °C	T_c, °C	χ_c, wt %	χ_c(PA6), wt %
100–0 ($\varepsilon = 0\%$)	53	221	190	28	-
60–40 ($\varepsilon = 0\%$)	78	217	170	15	26
0–100 ($\varepsilon = 0\%$)	124				

[a] It is noted that crystallinity values of PA6 largely depend on the characterization method, and DSC usually provides lower crystallinity values as compared to other methods.[30]

all PA6/aPA films. It has to be added that drawing temperature has no significant effect on the permeability. The effect of different morphological parameters, oxygen solubility, and molecular mobility on the permeability will be discussed below.

B. Thermal Properties of Films. The thermal characteristics of films are shown in Table 1. No crystallinity is detected in aPA film. The increase in the strain hardly influences the T_g of PA6 and PA6/aPA films. DSC traces of all PA6/aPA films show a single T_g similar to previous studies of PA6/aPA films.[40,52] The single T_g for PA6/aPA films suggests that under the used processing conditions PA6 and aPA are mixed on the scale of a few nanometers in the amorphous phase of these films. This result is in agreement with the prediction of mean-field binary model for blends of aliphatic polyamides with amorphous aromatic polyamides for the concentration used for preparation of films used for the present study.[53,54] The T_g of PA6/aPA film is seen to be ~25 °C higher than that of the PA6 film. This increase is expected and can be described by the Fox equation.[40]

Melting of PA6 in PA6/aPA films is observed at lower temperatures than in pure PA6 films, which is apparently caused by a decrease in crystal size and crystal perfection. Regarding the melting point depression in PA6/aPA films, it has been shown that it is related to a dilution effect of the aPA chains[26] rather than to transamidation of PA6 and aPA during melt processing.[55] The decrease in the crystallization temperature of PA6 in PA6/aPA films is also due to the reasons described above and the change of the local composition during crystallization.[56] As far as PA6 crystallinity in PA6/aPA films is concerned, the DSC results clearly show a decrease in the *overall* crystallinity, χ_c, with the addition of aPA. However, the crystal fraction per weight unit of PA6, χ_c(PA6), hardly changes in the presence of aPA.

C. Molecular Mobility by Low-Resolution ^{1}H NMR T_2 Relaxation. Analysis of proton NMR transverse magnetization relaxation (T_2 relaxation) is a valuable tool for analysis

of the phase composition in PA6.[30] It has been shown that the three-phase model provides the most appropriate description of the phase composition of PA6 fibers. The crystalline phase and a soft fraction of the amorphous phases are separated by an interfacial layer revealing chain mobility intermediate between that for the crystalline and less constrained (more mobile) soft amorphous fraction.[30] For determination of crystallinity, the measurement should be preferably performed at a temperature of 140 °C for dried samples. At this temperature, the crystalline phase, the semirigid crystal−amorphous interface and the soft amorphous fraction exhibit a significant difference in molecular mobility allowing reliable phase composition analysis. Despite exposure of samples to 140 °C, changes in the phase composition and molecular mobility due to annealing are negligible during the time required for the measurement, as has been shown by real-time NMR T_2 experiments for PA6 fibers.[30] For a range of structurally different PA6 fibers, it was found that crystallinity values, as determined by NMR, coincide within a few percent with the crystallinity determined using a rigorous method for PA6 fibers.[30] It will be shown below that changes in molecular mobility upon strain of PA6 films differ from that of the draw ratio used for the spinning of PA6 fibers. This is due to a difference in crystallinity during stretching of PA6 films and drawing of PA6 fibers. Comparison of NMR data for PA6 fibers and films, which will be provided below, could help us in better understanding the effect of processing conditions on molecular mobility and the phase composition of polyamide films and fibers.

Similar to PA6 fibers, the T_2 relaxation decay at 140 °C for unstretched PA6 film consists of the three T_2 relaxation components that are assigned to the crystalline phase (short relaxation time, T_2^s), semirigid crystal−amorphous interface (intermediate relaxation time, T_2^i), and soft fraction of the amorphous phase (long relaxation time, T_2^l) (Figure 2a). The relaxation times (T_2^{index}) provide information about molecular mobility. Longer relaxation time corresponds to larger frequency of chain motion, their amplitude, or both. The relative amount of the relaxation components, $\%T_2^s$, $\%T_2^i$, and $\%T_2^l$, represents the weight fraction of crystalline phase, semirigid crystal−amorphous interface, and soft fraction of amorphous phase in PA6 films, respectively.

The crystallinity of unstretched PA6 film is 54 wt %, which is within the common range of crystallinity of PA6 fibers.[30] The amount of the interface and the soft fraction of the amorphous phase in this film is 32 and 13 wt %, respectively. These values are also in the same range as observed for PA6 fibers.[30] It should be noted that the crystallinity of PA6, as determined by DSC (Table 1) and the NMR method, 28 and 54 wt %, respectively, largely differs due to the following reasons.[30] (1) Complex morphology of semicrystalline polymers requires different sets of assumptions for the analysis of data recorded by the different techniques. (2) Discrimination of the crystalline phase from the amorphous one is made on a basis of different characteristics, such as the enthalpy of melting (DSC), long-range periodicity (WAXD), bond vibrations (vibrational spectroscopy), the specific volume (density analysis), and molecular mobility (NMR relaxometry). For example, WAXD detects only large crystals consisting of several crystal unit cells, whereas NMR crystallinity includes both large and small nanosize crystals as well as disordered crystals. As far as the NMR crystallinity is concerned, the method determines the low mobile (rigid) mass fraction of semicrystalline polymers which is usually close to the crystallinity that is determined by traditional methods if the NMR

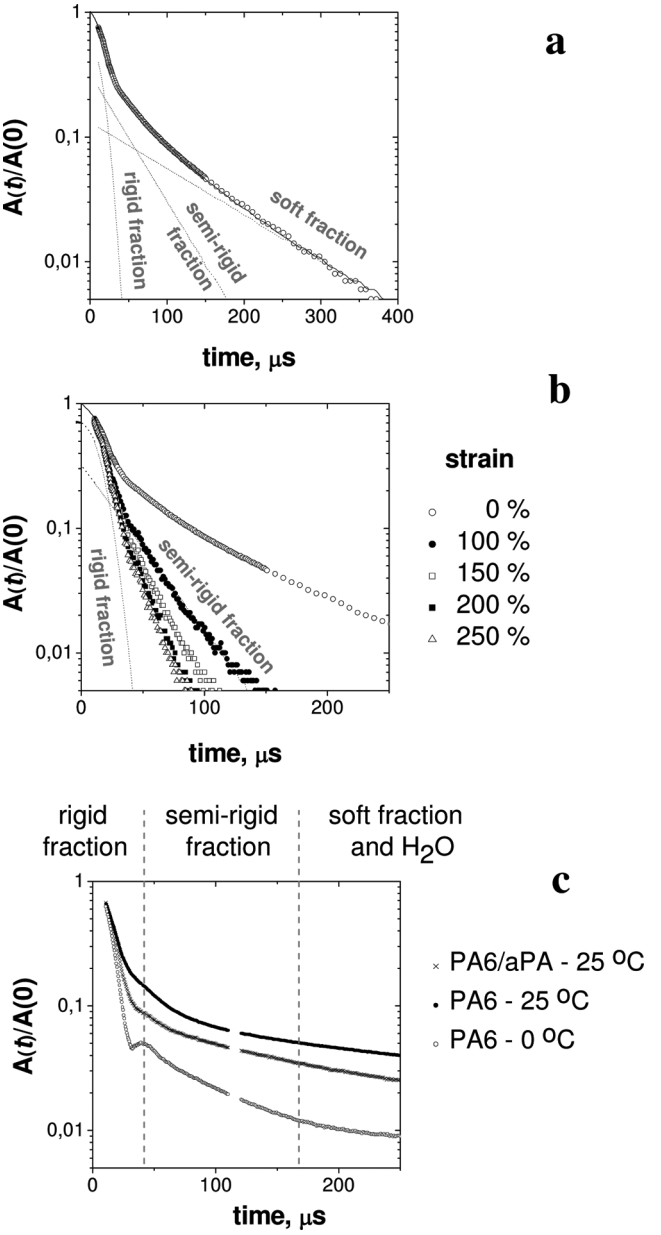

Figure 2. Proton NMR T_2 relaxation decay (FID) for dried unstretched (a) and stretched (b) PA6 films. The films were stretched at 100 °C. The FID's were measured at 140 °C using the 90° pulse excitation. The solid line represents the result of a least-squares adjustment of the FID (points) with a linear combination of the Gaussian and two exponential functions (see eq 1) for unstretched PA6 film (a). Dotted lines show the separate relaxation components which originate from polymer fractions with different molecular mobility for unstretched ($\varepsilon = 0\%$) (a) and stretched ($\varepsilon = 100\%$) (b) PA6 films. The total amplitude of the FID, $A(0) = A(0)^s + A(0)^i + A(0)^l$, was determined by a least-squares fit of the FID, and its value was normalized to 1. (c) FID for unstretched PA6 and PA6/aPA films at 23 °C and for PA6 film at 0 °C. The films were saturated with water at 23 °C and 85% relative humidity. Decay times, at which the T_2 relaxation is largely affected by molecular mobility in different fractions of films, are shown by dashed lines.

experiment is performed at temperatures much higher than the T_g of the amorphous phase. (3) The two-phase model, which is traditionally used for determining crystallinity, is rather simplified for describing semicrystalline polymers due to the presence of a crystal−amorphous interface, which can be detected either as a crystalline or amorphous fraction, depending on the method used. In other words, where is the

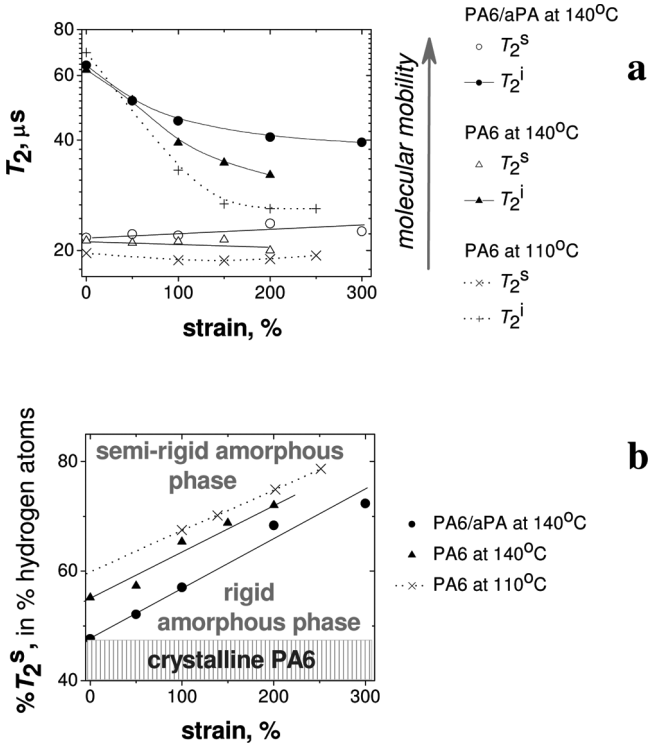

Figure 3. (a) Proton T_2 relaxation time for rigid (T_2^s) and semirigid (T_2^i) fractions of dried PA6 and PA6/aPA films. The films were stretched at 100 °C. The T_2 relaxation times were measured at 110 and 140 °C for PA6 films and at 140 °C for PA6/aPA films. (b) The relative amount of rigid fraction, as determined by the hydrogen content in this fraction ($\%T_2^s$). The two-component analysis of the T_2 decay was used for determining the amount of the semirigid amorphous fraction in all films. The rigid fraction is composed of crystalline PA6 and rigid amorphous fractions as shown in this figure.

borderline between crystalline and amorphous phases in terms of physical properties as measured by different methods? Various experimental methods, such as WAXD, neutron scattering, dielectric relaxation, calorimetry, solid-state NMR, and molecular modeling, show that a thin layer separates crystalline and amorphous phases, and the properties of this layer are intermediate between those of crystalline and amorphous phases. The term "rigid amorphous phase" has been also discussed in this respect.

In addition to the T_2 relaxation analysis at 140 °C for dried films, the T_2 relaxation decay was also recorded at 23 and 0 °C for unstretched PA6 and PA6/aPA films which were saturated with water (23 °C/85% RH) (Figure 2c). These experiments were performed because oxygen permeability was determined for wet films at 23 °C. Chain mobility at 23 °C in the amorphous phase of wet films is lower as compared to that in dry films at 140 °C as could be seen by comparing the T_2 relaxation decays for unstretched dry and wet PA6 films at 140 and 23 °C, respectively (Figures 2a and 2c). However, a fraction of the amorphous phase in wet PA6 and PA6/aPA flms is still mobile at 23 °C. A small fraction of the amorphous phase in wet PA6 film is still mobile at 0 °C.

Stretching of PA6 films causes large decrease in molecular mobility, as can be seen from the results in Figures 2b and 3. Stretching causes disappearance of the soft fraction of the amorphous phase which is already transformed to a semirigid amorphous fraction at 100% strain, as can be seen in Figure 2b. In addition, molecular mobility in the semirigid fraction decreases upon increasing strain too (Figure 3a). The amount of rigid fraction in PA6 films increases from 54 to 72 wt % proportionally to the strain (Figure 3b). This increase can be due to an increase in crystallinity, similar to the effect of draw ratio for PA6 fibers,[30] and/or due to immobilization of highly stretched chain fragments in the interface and possibly in the amorphous phase. DSC and X-ray studies of PA6 films have shown that the crystallinity is hardly affected by the strain.[57,58] Therefore, it can be concluded that the increase in the amount of the rigid fraction is mainly related to strain-induced immobilization of the crystal−amorphous interface and some chain fragments in the amorphous phase. Approximately 40% of the noncrystalline phase of the PA6 film is largely immobilized at 200% strain. At the time scale of the NMR method (approximately tens of microseconds), chain mobility in this noncrystalline fraction is largely suppressed and is similar to that of the glassy polymer.

The stretching-induced immobilization of the noncrystalline phase of PA6 films differs from the effect of draw ratio on molecular mobility in the amorphous phase of PA6 fibers.[30] Contrary to PA6 fibers, molecular mobility in the noncrystalline phase of PA6 films largely decreases with increasing strain. This difference in immobilization of the amorphous phase upon stretching of PA6 films, as compared to drawing of PA6 fibers, is due to differences in the degree of crystallinity of PA6 films and fibers at the moment when the materials are stretched. Because of very fast cooling of fiber filaments during fiber spinning, the process of cold crystallization takes place predominantly during or after winding of spun fibers when the fiber absorbs moisture from the surrounding air and the T_g drops below room temperature.[30] In contrast to PA6 fibers, molten PA6 crystallizes upon fast cooling on a chill roll at 100 °C, and the films were annealed at 110 °C before the films are stretched. Stretching of polyamide films in a semicrystalline state causes high elongation of chain fragments in the amorphous phase, since crystallites act as physical network junctions. At this point the difference between chain elongation and chain orientation should be mentioned. Chains can be highly elongated without any preferential orientation. For example, chains in polymer networks are highly elongated at the equilibrium swollen state, whereas the order parameter is zero. The chain elongation and topological constraints from crystallites cause large anisotropy of chain motion as detected by a large decrease in the T_2^i of the amorphous phase (Figure 3a). It should be mentioned that the effect of chain elongation (the strain-induced anisotropy of molecular motions) on T_2 is well established for deformed rubbery materials.[59−63]

In the discussion below, the permeability of PA6/aPA films will be compared with that of PA6 films. Since the T_g of PA6/aPA films is ~25 °C higher than the T_g of PA6 (Table 1), the NMR experiments for PA6 films are performed not only at 140 °C but also at 110 °C. The results for PA6 at 110 °C will allow us to compare the molecular mobility in both types of films at approximately the same temperature above T_g. Upon decreasing the temperature from 140 to 110 °C, the amount of rigid fraction in PA6 films increases due to the immobilization of more constrained chain fragments in the amorphous phase (Figure 3b).[30] Moreover, molecular mobility of less constrained chain fragments in the amorphous phase decreases, too (Figure 3a).

The amount of rigid fraction (in % hydrogen atoms) at 140 °C in unstretched PA6/aPA film is smaller than in unstretched PA6 film at 110 °C due to the presence of amorphous polyamide in the blend (Figure 3b). The degree of crystallinity of PA6 (in wt %) in unstretched PA6/aPA film can be estimated from $\%T_2^s$ using the known percentage of hydrogen atoms in PA6 and aPA, the sample composition, and assuming that the majority of aPA chain fragments are

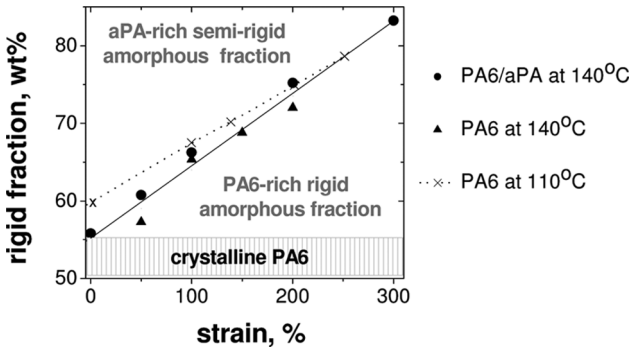

Figure 4. Amount of rigid fraction (in wt %) in dried PA6 and PA6/aPA films versus strain used for film preparation. The films were stretched at 100 °C. The two-component analysis of the T_2 decay was used for determining the amount of rigid fraction in all films. The rigid fraction is composed of crystalline PA6 and rigid amorphous fractions as shown in this figure.

not immobilized by trapping in rigid domains of PA6. This suggestion is confirmed by the ^{13}C NMR IRCP experiment discussed below. With these assumptions, the crystallinity of PA6 in unstretched PA6/aPA film is determined to be approximately the same as in unstretched PA6 film, i.e., 54 wt % (Figure 4). The same crystallinity of PA6 in both types of film was also shown by DSC (Table 1). Thus, the mobile fraction of the amorphous phase of PA6/aPA films is enhanced by aPA, as shown schematically in Figure 5.

The stretching of PA6/aPA films causes a significant increase in the amount of rigid fraction, similar to that for PA6 films (Figure 4). Despite the high amount of amorphous aPA in the amorphous phase of PA6/aPA films, molecular mobility in the semirigid fraction of PA6/aPA films at 140 °C is also largely hindered and is only slightly larger than that in PA6 films, as can be seen in Figure 3a. This suggests that aPA chains are also largely elongated upon stretching of PA6/aPA films, similar to that of PA6 chains. Elongation of aPA chains in PA6/aPA films could find the following explanation. It is known that free chains, solvent, and oligomer molecules in a deformed polymer network reveal strain-induced orientation, which may be due to either enthalpic or entropic origin.[64,65] The coupling in elongation of PA6 and aPA chains in the stretched polyamide films should be even more pronounced due to hydrogen bond formation between amide groups of PA6 and aPA chains, small amount of chain entanglements, and most probubly due to the formation of copolymers caused by transamidation which could occur during melt processing.

D. Partitioning of PA6 and aPA Chain Units between Rigid and Semirigid Amorphous Fractions of PA6/aPA Film. The ^{13}C NMR IRCP experiments are very sensitive to the local proton environment and to the heterogeneity of molecular motion.[66−69] In this experiment, the ^{13}C NMR transverse magnetization is first created during a relatively long cross-polarization time, τ_{cp}, and is than inverted during an inversion time, τ_{in}. The main advantage of this experiment, as compared to conventional ^{13}C NMR methods, is the following. The amplitude of the spectra lines is positive at short τ_{in}. An increase in τ_{in} causes a phase inversion of the magnetization. As a result of that line intensities decrease and become negative at longer τ_{in}. The inversion time, the time at which the intensity become negative, τ_{in}^{zero}, is longer for less protonated carbon atoms (proton poor local environment) and for more mobile molecular species. Thus, the experiment allows easy visualization of the differences in molecular mobility for the same type of carbon atoms, especially in the case of strongly overlapping spectral lines.[69]

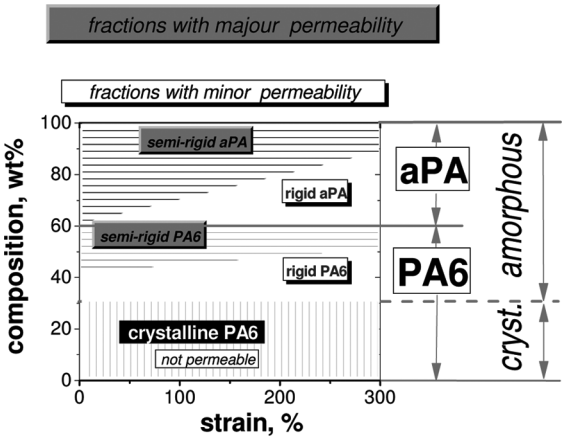

Figure 5. Schematic drawing of the phase composition in PA6/aPA films at temperatures well above T_g as a function of strain used for film preparation. Difference in permeability of crystalline phase, rigid, and semirigid amorphous fractions is indicated by black, white, and gray text bars, respectively.

^{13}C NMR CPMAS spectra ($\tau_{in} = 0$) of unstretched films were recorded at temperatures above T_g, i.e., at 110 and 130 °C for dried PA6 and PA6/aPA films, respectively. The spectrum of the PA6 film shows resonances of aliphatic carbon atoms in the spectra range from 26 to 43 ppm and carbonyl carbon at ~173 ppm.[70,71] In addition to these resonances, the ^{13}C NMR CPMAS spectrum of PA6/aPA film shows resonances in the range of 127−137 ppm originating from aromatic carbon atoms and a line at ~168 ppm from the carbonyl atom adjacent to the aromatic ring of aPA.[56] Upon increasing τ_{in}, τ_{in}^{zero} is observed at the following τ_{in}: 40−60 μs for aliphatic carbon atoms of PA6/aPA and those in crystalline and amorphous phases of PA6, 70−360 μs for aromatic carbons of aPA, and 400−500 μs for carbonyl carbons. No large difference in τ_{in}^{zero} is observed for crystalline and amorphous phases of PA6. This means that molecular mobility in these phases does not significantly differ at temperatures largely exceeding T_g. Thus, molecular mobility in the amorphous phase of both films is largely restricted. This is in agreement with ^{1}H T_2 results as can be concluded from small difference between T_2^s and T_2^i values (Figure 3a) as compared to that for PA6 fibers.[30]

Qualitative information about partitioning of aPA chains between rigid and semirigid amorphous fractions in the PA6/aPA film is provided by comparing the inversion behavior of carbonyl resonances. If PA6 and aPA would be mixed in the amorphous phase on the molecular scale, one could expect nearly the same inversion time for carbonyl atoms of both nylons in PA6/aPA film. Figure 6 shows ^{13}C NMR IRCP spectra for unstretched PA6/aPA film at a few selected values of τ_{in}. The inversion of carbonyl resonances is observed at τ_{in} of approximately 400−430 μs and at $\tau_{in} > 460$ μs for PA6 and aPA, respectively. Resonances of carbon atoms of the same chemical origin and in the same local proton environment should have longer inversion times in the case of higher molecular mobility. Thus, results of the ^{13}C NMR IRCP experiment show that the composition of the semirigid (more mobile) amorphous fraction in unstretched PA6/aPA film is enhanced by aPA. This conclusion does not contradict to DSC data showing a single glass transition temperature for PA6/aPA films due to differences in the length scale of heterogeneity determined by these two methods. The NMR method probes dynamical heterogeneity on the subnanometer level, contrary to DSC which determines different T_g in blends if the dimensions of phase-separated domains exceed a few nanometers.

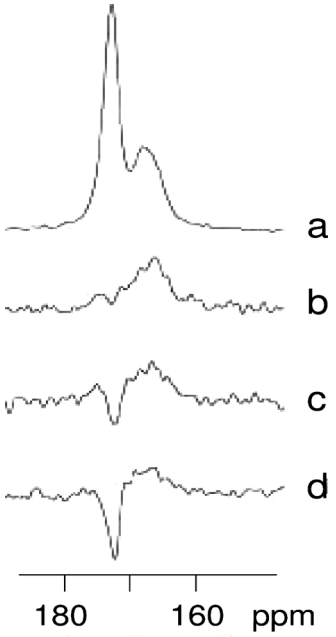

Figure 6. Evolution of carbonyl resonances in ^{13}C NMR IRCP spectra for dried unstretched PA6/aPA film upon increasing inversion time τ_{in}: $\tau_{in} = 0$ (a), 400 (b), 430 (c), and 460 μs (d). The amplitude of the spectra lines is magnified by 5 times at $\tau_{in} \geq 400$ μs. The spectra were recorded at 130 °C.

E. Domain Sizes by Different Methods. An AFM study of PA6 films has shown that three to four lamellae form stacks of uniform size with a width/thickness ratio of about three.[72] The morphology of PA6 and PA6/aPA films, which have been prepared at DSM using similar conditions, were studied by X-ray and AFM.[40,52,72,73] The lamellar thickness in all films equals 6 ± 1 nm regardless of the strain used, as shown by AFM.[52] X-ray study of uniaxially stretched PA6 films has revealed that the dimensions of crystallites are not largely affected by film processing conditions.[74] The lamellar thickness in PA6 fibers is also in the range of 4−6 nm.[44] Apparently, the lamellar thickness in PA6 films and fibers is not largely affected by processing conditions. As far as typical lamellar width in PA6 films is concerned, it equals ~20 nm.[75] The thickness of interlamellar amorphous layers in similar PA6 films is in the range of 2−3 nm, and its value is not largely affected by the strain, as has been shown by proton NMR spin-diffusion experiments.[76] Thus, it can be concluded that the aspect ratio of crystallites in polyamide films is small.

F. Oxygen Solubility in PA6 and PA6/aPA Films. Oxygen solubility in semicrystalline polymers depends on the chemical structure of polymers, morphology, and several physical properties which are influenced by processing conditions and thermal history of the material. Therefore, knowledge of differences in oxygen solubility in a series of samples is needed for determining factors influencing the permeability. Analysis of oxygen flux through polymer films is generally used for determining the apparent diffusion coefficient and oxygen solubility values which are specific for each film processed at certain conditions.[29,51,77,78] In the present study, the relative difference in oxygen solubility in PA6 and PA6/aPA films is determined by proton NMR spin−lattice (T_1) magnetization relaxation experiments. Oxygen absorbed by polymers causes a decrease in T_1 relaxation time of the polymer as compared to a well-degassed specimen of the polymer.[79,80] A decrease in T_1 depends on the amount of absorbed oxygen and its mobility.

The temperature dependence of proton T_1 relaxation time for unstretched PA6 and PA6/aPA films is compared for the samples under dry air and nitrogen atmosphere (Figure 7a,b) as well as for the films saturated with water (23 °C/85% RH) under air (Figure 7c,d). The T_1 value for dried films shows a minimum at ~0 °C. The minimum, which is caused by molecular motions with frequency of ~20 MHz, can be assigned to a subglass transition motion of CH_2 groups in agreement with lower frequency dielectric spectroscopy,[81,82] solid-state NMR,[42] and DSC[83] studies. The T_1 increases upon temperature decrease due to a decrease in the frequency and/or amplitude of the molecular motions. The T_1 value for PA6 and PA6/aPA films under a dry nitrogen atmosphere is nearly the same at low temperatures. This suggests that subglass transition dynamics of aliphatic chain segments is similar in both types of films. In the presence of oxygen, T_1 values are lower than their values for films under nitrogen. The decrease is larger for PA6/aPA films than for PA6 film.

At low concentrations of paramagnetic impurities,[84−86] such as oxygen molecules, the contribution of oxygen molecules to the overall T_1 relaxation, T_1^{oxygen}, can be provided by the following equation: $(T_1^{oxygen})^{-1} = (T_1^{air})^{-1} - (T_1^{nitrogen})^{-1}$, where T_1^{air} and $T_1^{nitrogen}$ are T_1 relaxation times of films under air and nitrogen atmosphere, respectively. T_1^{oxygen} decreases proportionally to the amount of oxygen absorbed by the films. This equation is applicable in the case of fast spin-diffusion through the sample volume, which is the present case as it follows from the single-exponential T_1 relaxation process observed. The T_1^{oxygen} value can be used for determining relative differences in oxygen solubility because (1) local mobility of polyamide chains in both samples is nearly the same because $T_1^{nitrogen}$ values are approximately the same for both films and (2) molecular mobility of oxygen molecules in both films could also be comparable due to similar chain mobility in the host matrix in both films. It could be suggested that the relative difference in oxygen solubility between films is not largely affected by temperatures below T_g. The T_1^{oxygen} is approximately 1.5−2 times shorter for PA6/aPA film than for PA6 films. Thus, oxygen solubility in dried PA6/aPA film is larger than in dried PA6 films. The T_1 experiments for dried PA6 films stretched to ε of 200% reveal slightly lower oxygen solubility than in unstretched PA6 film.

Since oxygen permeability was measured for films saturated with water, the effect of absorbed water on the T_1 relaxation and, consequently, on oxygen solubility was studied for the same films after they were saturated with water under an air atmosphere. Water plasticizes the amorphous phase causing a decrease in the glass transition temperature (T_g) from 53 °C for dried PA6 film to a temperature well below room temperature.[48] Above ≈−30 °C, the T_1 relaxation time of the films with absorbed water is shorter than that of the dried films due to the lowering of T_g upon water uptake. At lower temperatures, films with absorbed water have longer T_1 as compared to T_1 of dried films under air (Figure 7c,d). This suggests lower oxygen solubility due to a competition of water molecules with the permeant gas for free volume excess in the amorphous phase, thereby reducing oxygen solubility.[48−51] The relative decrease in oxygen solubility is nearly the same in PA6 and PA6/aPA films, which are saturated with water, as could be concluded from similar $T_1^{oxygen}(H_2O)$ values for both films (Figure 7c,d). Thus, oxygen solubility in dried and wet (23 °C/85% RH) PA6/aPA film is larger than that in PA6 film. Greater oxygen solubility in PA6/aPA film could be caused by specific interaction of oxygen molecules with aromatic rings of aPA, as will be discussed below.

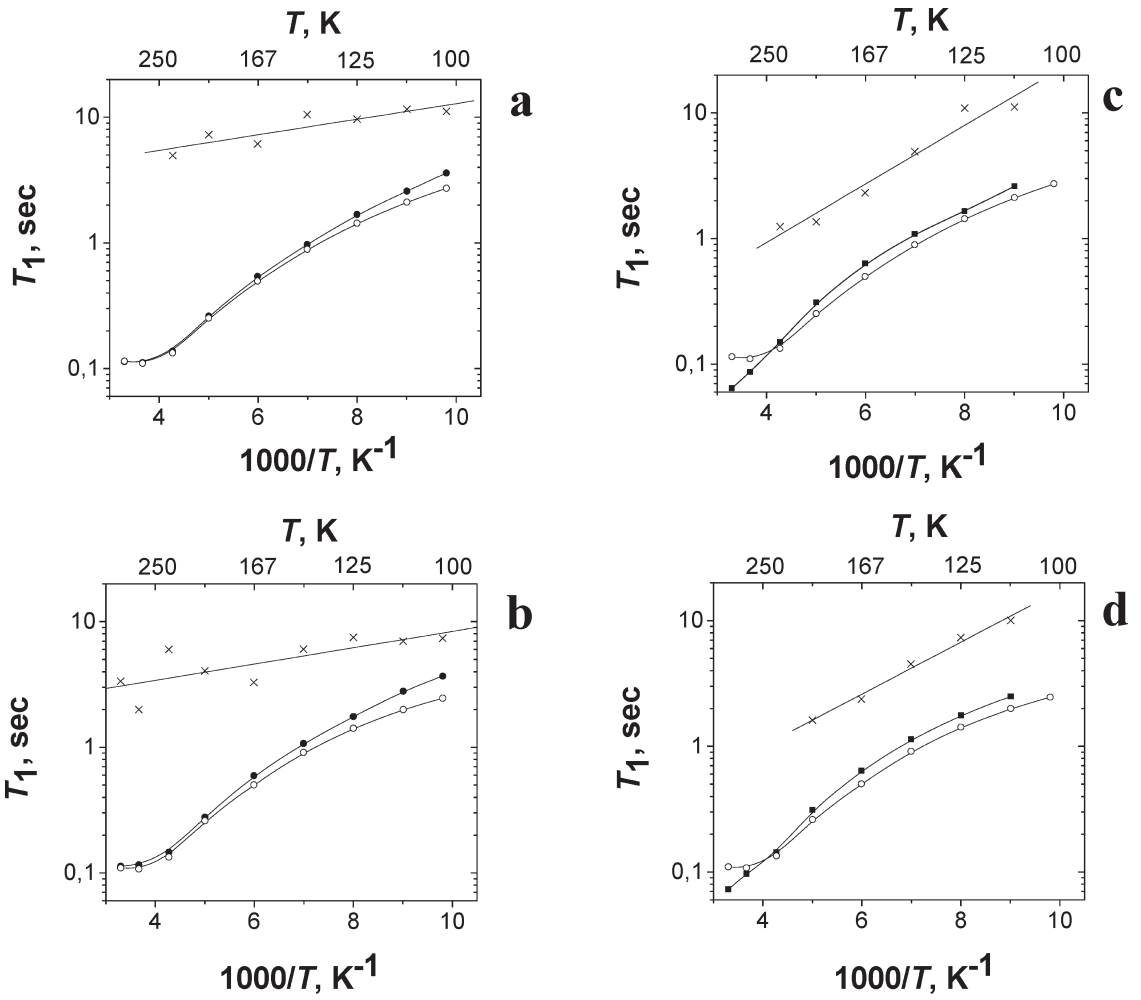

Figure 7. (a, b) Temperature dependence of proton T_1 relaxation time of unstretched PA6 (a) and PA6/aPA (b) films under dry nitrogen (closed circles) and dry air (open circles). Chill roll temperature, which was used for film processing, was 100 °C. Lines are a guide to the eye. Contribution of paramagnetic oxygen (T_1^{oxygen}) to T_1 relaxation of films under air is shown by crosses. The straight line represents the result of a linear regression analysis of the temperature dependence of T_1^{oxygen} for (a) PA6 film: intercept = 0.49 ± 0.10 s, slope = 0.062 ± 0.014 s/K, coefficient of determination = 0.89 and for (b) PA6/aPA film: intercept = 0.27 ± 0.14 s, slope = 0.065 ± 0.020 s/K, coefficient of determination = 0.77. (c, d) The dependence of proton T_1 relaxation time on temperature for unstretched PA6 (c) and PA6/aPA (d) films, which are saturated with water under air atmosphere (closed squares). T_1 values for the films under dry air (open circles) are shown in (c, d) for comparison. The relative decrease in oxygen solubility upon water absorption $[T_1^{oxygen}(H_2O)]$ is shown by crosses. $[T_1^{oxygen}(H_2O)]$ is determined as follows: $[T_1^{oxygen}(H_2O)]^{-1} = [T_1^{oxygen}(\text{dry air})]^{-1} - [T_1^{oxygen}(H_2O)]^{-1}$. The straight line represents the result of a linear regression analysis of the temperature dependence of $[T_1^{oxygen}(H_2O)]$ for (c) PA6 film: intercept = −0.96 ± 0.17 s, slope = 0.23 ± 0.03 s/K, coefficient of determination = 0.98 and for (d) PA6/aPA film: intercept = −0.83 ± 0.09 s, slope = 0.21 ± 0.02 s/K, coefficient of determination = 0.99.

IV. Discussion

The effect of the following molecular and morphological characteristics of PA6 and PA6/aPA films will be discussed below in relation to oxygen permeability of the films: (1) crystallinity and the amount of crystalline polymorphs, (2) lamellar thickness, (3) aspect ratio of crystal lamellae and lamellae stacks, (4) crystal orientation, (5) the amount of rigid amorphous fraction, (6) molecular mobility and chain orientation in the amorphous phase, and (7) oxygen solubility and specific interactions of oxygen molecules with polymer chains. It should be mentioned that upon stretching several of these structural parameters change in very close relation to each another. For example, strain-induced orientation in the amorphous phase hinders molecular mobility, affects oxygen solubility,[25] and causes anisotropy of the diffusion rate relative to the orientation direction.[87−90]

A. PA6 Films. The crystallinity of PA6 films is nearly the same in all films as determined by DSC study of the samples.[40] Differences in the relative amount of crystalline polymorphs of PA6 in the films will not influence the permeability since it is anticipated that crystalline regions of PA6 are not accessible for oxygen molecules. The lamellar thickness and the mean thickness of amorphous domains are hardly affected by strain, as discussed above. The aspect ratio of lamellar stacks that are formed by three to four lamellae is small, as has been shown by previous AFM studies of PA6 films prepared at DSM in a similar manner.[40,91,92] Despite the fact that crystal orientation increases with increasing strain, no large differences in the orientation are observed between unstretched and stretched PA6 films, as determined by X-ray study of similar polyamide films prepared at DSM.[40] Since there are no substantial differences in crystallinity, semicrystalline morphology and small aspect ratio of lamellar stacks in the series of PA6 films studied, we suggest that these characteristics would not largely affect the tortuosity factor as a function of strain. Therefore, differences in oxygen permeabilitity of PA6 films (Figure 1) should be determined by structural changes in the amorphous phase that are induced by film stretching, namely chain orientation and immobilization of the amorphous phase. Both these parameters affect oxygen solubility[93] and self-diffusion of

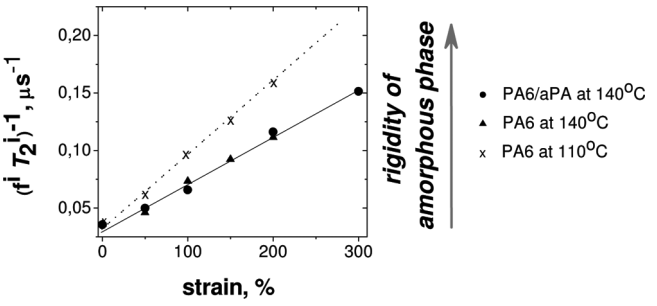

Figure 8. Effect of strain on the parameter *SA* characterizing strain-induced immobilization (rigidity) of the amorphous phase in dried PA6 and PA6/aPA films. The films were stretched at 100 °C. The parameter *SA* is reciprocal product of $T_2{}^i$ relaxation time (in μs), which characterizes molecular mobility in the semirigid (more mobile) fraction of the amorphous phase, and the amount of the semirigid amorphous fraction (f^i): $SA = (f^i T_2)^{-1}$, where $f^i + f^s = 1$ (see eq 1). Lines represent the result of a linear regression analysis of the dependence of *SA* on strain for PA6 films at 140 °C: intercept = $0.031 \pm 0.003\ \mu s^{-1}$, slope = $(4.0 \pm 0.2) \times 10^{-4}\ \mu s^{-1}$, coefficient of determination = 0.997; for PA6/aPA films at 140 °C: intercept = $0.032 \pm 0.003\ \mu s^{-1}$, slope = $(4.0 \pm 0.3) \times 10^{-4}\ \mu s^{-1}$, coefficient of determination = 0.993; and for PA6 films at 110 °C: intercept = $0.032 \pm 0.008\ \mu s^{-1}$, slope = $(6.5 \pm 0.5) \times 10^{-4}\ \mu s^{-1}$, coefficient of determination = 0.993.

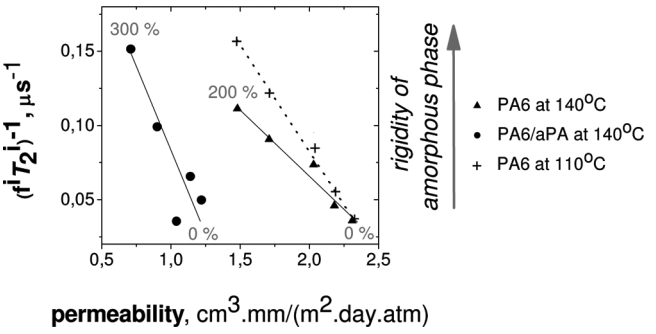

Figure 9. Parameter $SA = (f^i T_2{}^i)^{-1}$, which characterizes strain-induced immobilization (rigidity) of the amorphous phase in dried films, versus oxygen permeability of PA6 and PA6/aPA films. The films are stretched at 100 °C. The permeability was measured at 23 °C and 85% relative humidity. The minimum and maximum strains of films are shown in the figure. In order to determine the effect of different T_g of PA6 and PA6/aPA films on the *SA* parameter, the *SA* values for PA6 are shown at 110 and 140 °C.

oxygen in the amorphous phase. Diffusivity largely decreases with decreasing molecular mobility, i.e., the diffusion coefficient of small molecules in rigid polymers is ~2 orders of magnitude smaller than that in rubbery materials.[8] Chain orientation in the amorphous phase, which is accompanied by a decrease in chain mobility, also causes a decrease in oxygen solubility, as has been demonstrated for polyester[25,26] and polypropylene[93] films.

Two parameters that characterize molecular mobility in the amorphous phase are important for better understanding film permeability, namely the amount of semirigid amorphous fraction—the fraction with less constrained (more mobile) chain fragments—and molecular mobility in this amorphous fraction. Permeability should decrease with increase in the amount of rigid amorphous fraction due to an increase in the diffusion path and a decrease in oxygen solubility. The diffusion rate of oxygen molecules should decrease with decreasing chain mobility in the semirigid amorphous fraction. Thus, a decrease both in the amount of more mobile amorphous fraction and in molecular mobility in this fraction should cause a decrease in permeability. Therefore, we introduced a parameter *SA* (soft amorphous fraction) that describes the rigidity of the amorphous phase. The parameter is the reciprocal product of the T_2 relaxation time of the semirigid (more mobile) fraction of the amorphous phase ($T_2{}^i$ in μs) and its amount (f^i): $SA = (f^i T_2{}^i)^{-1}$, where $f^i = A(0)^i/[A(0)^s + A(0)^i]$ (see eq 1) and $f^s + f^i = 1$. An increase of this parameter corresponds to overall strain-induced immobilization of the amorphous phase—increase in its rigidity. Both increase in film strain and decrease in temperature cause immobilization of the amorphous phase, as can be seen in Figure 8. It is remarkable that the dependence of the *SA* on strains is the same for PA6 and PA6/aPA films at 140 °C.

In general, one should expect a decrease in permeability with increasing the *SA*. In order to establish the role of molecular mobility in the amorphous phase on transport properties, the rigidity parameter *SA* was compared with oxygen permeability in Figure 9. The NMR data for PA6 films were determined for dried films at 110 and 140 °C. This temperature is approximately 50−80 °C above the T_g. The permeability values, which are shown in Figure 9, were measured for PA6 and PA6/aPA films at 85% humidity and 23 °C. This temperature is also above T_g of unstretched PA6 and PA6/aPA films as shown above (Figure 2c). It is well established that the temperature dependence of the diffusion coefficient of small molecules in polymers displays behavior very similar to the temperature dependence of chain mobility corresponding to glass transition.[94] Since both the *SA* and the permeability were determined at temperatures above T_g, we can compare these two characteristics assuming the validity of the time−temperature superposition principle.

The dependence in Figure 9 shows a clear trend, namely, that the permeability decreases proportionally to the increase in the rigidity of the amorphous phase as determined by the *SA* parameter. Therefore, we can suggest that the semirigid (more mobile) fraction of the amorphous phase in stretched films plays a crucial role in transport properties and this fraction could be considered as "channels" for diffusion of gas molecules. The increase in the amount of more mobile amorphous fraction as well as in molecular mobility in this fraction results in an increase in both diffusivity and solubility of oxygen molecules. Thus, the results for PA6 films show that the *SA* parameter which describes rigidity of the amorphous phase can be used for determining the relative difference in permeability of small molecules in a series of samples of similar origin.

B. PA6/aPA Films. Strain-induced immobilization of the amorphous phase in PA6/aPA films, as characterized by the *SA* value, is similar to that for PA6 films (Figure 8). This similarity suggests that immobilization of aPA and PA6 chain fragments in the amorphous phase is comparable due to the reasons discussed above. Despite lower overall crystallinity in PA6/aPA films (Table 1), the amount of rigid fraction, which is composed of crystalline PA6 and rigid amorphous phase, is nearly the same for both types of films stretched to the same ε (Figure 4).

Similar to PA6 films, the permeability of unstretched PA6/aPA films decreases proportionally to the increase in the rigidity of the amorphous phase as defined by the *SA* parameter (Figure 9). The permeability of PA6/aPA film is significantly lower than its value for all PA6 films. Since some fraction of the amorphous phase is mobile at 23 °C in unstretched water-saturated PA6 and PA6/aPA films, this means that in addition to molecular mobility in the amorphous phase oxygen solubility as well as specific interactions between polymer chains and oxygen molecules plays an important role in the permeability.

Oxygen solubility in PA6/aPA films is larger than in PA6 films as was concluded from results of ^1H T_1 relaxation experiments discussed above. Therefore, lower permeability of PA6/aPA films suggests that specific interactions between oxygen molecules and aromatic rings of aPA can play a role in slowing down oxygen diffusivity. A previous study of syndiotactic polystyrenes (*s*-PS) has shown that oxygen molecules are selectively adsorbed on aromatic rings.[95] The activation energy for complex formation between aromatic rings of *s*-PS and oxygen molecules is 10−16 kJ/mol,[95] and ∼6 kJ/mol for the complex between benzene and O_2, as has been shown by *ab initio* calculations[96] and an UV spectroscopic study.[97] The formation of charge-transfer complexes between aromatic rings and oxygen molecules has been observed for several compounds.[98−101] The interaction of oxygen with aromatic polymers also influences molecular mobility of polymer chains.[98,102] The effect of specific interactions on a decrease in diffusivity of small molecules in (bio)polymers is well established.[9,103−106] The model proposed assumes that small molecules are "bound" for a certain fraction of time to larger and less mobile molecules. The meaning of "bound" should not be taken too literally. An exchange occurs between "bound" and free states of molecules. The stronger the interactions regardless of their type, the longer is the residence time of small molecules in the "bound" state and the slower the diffusion is. Similar to that, specific interactions of oxygen molecules with aromatic rings of PA6/aPA can cause a decrease in oxygen diffusivity. It was shown above that the composition of mobile amorphous fraction, which plays a major role in the permeability, is largely enhanced by aPA in PA6/aPA film. Thus, the specific interaction between oxygen molecules and aromatic rings of aPA can explain lower oxygen permeability of PA6/aPA films as compared to PA6 films as well as the higher gas barrier property of aromatic polyamides as compared to aliphatic ones.[50]

V. Conclusions

The present study reveals the important role of molecular mobility in the amorphous phase on the permeability of polyamides films. It is shown that immobilization of the amorphous phase largely depends on the stretching degree of films, although crystallinity of PA6 in PA6 and PA6/aPA films is hardly affected by the strain that was used for film preparation. A significant amount of the amorphous phase in both types of films is rigid at temperatures above 100 °C, similar to the amorphous phase of PA6 in the glassy state. The amount of rigid amorphous fraction increases proportionally to the strain due to strain-induced elongation of chain fragments in the amorphous phase. Molecular mobility in the remaining semirigid amorphous fraction is largely restricted even at temperatures well above T_g and decreases upon strain. The composition of this amorphous fraction in PA6/aPA films is enhanced by aPA. It is suggested that the semirigid fraction of the amorphous phase in stretched films could be considered as "channels" for diffusion of gas molecules. Therefore, knowledge of the two parameters characterizing molecular mobility in the amorphous phase, i.e. the amount of the semirigid (more mobile) fraction of the amorphous phase and molecular mobility in this fraction, is important for better understanding of film permeability. Both a decrease in the amount of the semirigid fraction and molecular mobility in this fraction cause a significant decrease in oxygen permeability of polyamide films. In addition to molecular mobility, the specific interactions between aromatic rings of aPA and oxygen molecules play an important role in the permeability of these types of polymer films. Although oxygen solubility in PA6/aPA films is larger than that in PA6 films, the complex formation between aromatic rings of aPA and oxygen molecules slows down oxygen diffusivity. Results of the present study are of interest for a better understanding of both permeability of polyamide films and other phenomena in polymers that are affected by transport properties of small molecules, such as the rate of water uptake, dyeability of fibers, and thermal oxidation.

Acknowledgment. The authors thank Angelika Schmidt for discussions at an early stage of this study, Marnix van Gurp and Chris Duxbury for comments on the manuscript, and Petra Ramakers for performing permeability experiments.

References and Notes

(1) Weinkauf, D. H.; Paul, D. R. In *Barrier Polymers and Structures*; Koros, W. J., Ed.; ACS Symposium Series 423; American Chemical Society: Washington, DC, 1990; p 60.
(2) Bharadwaj, R. K. *Macromolecules* **2001**, *34*, 9189.
(3) Gelfer, M. Y.; Waddon, A.; Schmidt-Rohr, K.; Gale, R.; Kleiner, L.; Berggren, R. *J. Polym. Sci., Part B: Polym. Phys.* **2001**, *39*, 2774.
(4) Yamamoto, T.; Kanda, T.; Nishihara, Y.; Ooshima, T.; Saito, Y. *J. Polym. Sci., Part B: Polym. Phys.* **2009**, *47*, 1181.
(5) Karayiannis, N. Ch.; Mavrantzas, V. G.; Theodorou, D. N. *Macromolecules* **2004**, *37*, 2978.
(6) Rogers, C. E. In *Polymer Permeability*; Comyn, J., Ed.; Elsevier Applied Science: London, 1985; p 11.
(7) Duda, J. L.; Zielinski, J. M. In *Diffusion in Polymers*; Neogi, P., Ed.; Marcel Dekker: New York, 1996; p 143.
(8) Koros, W. J. In *Barrier Polymers and Structures*; Koros, W. J., Ed.; ACS Symposium Series 423; American Chemical Society: Washington, DC, 1990; p 1.
(9) Tomić, K.; Veeman, W. S.; Boerakker, M.; Litvinov, V. M.; Dias, A. A. *J. Pharm. Sci.* **2008**, *97*, 3245.
(10) Litvinov, V. M. *Macromolecules* **2006**, *39*, 8727.
(11) Barrer, R. M.; Skirrow, G. *J. Polym. Sci.* **1948**, *3*, 549, 564.
(12) Stern, S. A.; Trohalaki, S. In *Barrier Polymers and Structures*; Koros, W. J., Ed.; ACS Symposium Series 423; American Chemical Society: Washington, DC, 1990; p 22.
(13) Theodorou, D. N. In *Diffusion in Polymers*; Neogi, P., Ed.; Marcel Dekker: New York, 1996; p 67.
(14) Isasi, J. R.; Mandelkern, L.; Galante, M. J.; Alamo, R. G. *J. Polym. Sci., Polym. Phys. Ed.* **1999**, *37*, 323.
(15) Mendelkern, L. *Acc. Chem. Res.* **1990**, *23*, 380.
(16) Baker, A. M. E.; Windle, A. H. *Polymer* **2001**, *42*, 667.
(17) Hiss, R.; Hobeika, S.; Lynn, C.; Strobl, G. *Macromolecules* **1999**, *32*, 4390.
(18) Iwata, K. *Polymer* **2002**, *43*, 6609.
(19) Sajkiewicz, P.; Hashimoto, T.; Saijo, K.; Gradys, A. *Polymer* **2005**, *46*, 513.
(20) Schick, C.; Wurm, A.; Mohammed, A. *Thermochim. Acta* **2003**, *396*, 119.
(21) Xu, H.; Cebe, P. *Macromolecules* **2004**, *37*, 2797.
(22) Androsch, R.; Wunderlich, B. *Polymer* **2005**, *46*, 12556.
(23) Menczel, J. D.; Jaffe, M. *J. Therm. Anal. Calorim.* **2007**, *89*, 357.
(24) Zia, Q.; Mileve, D.; Androsch, R. *Macromolecules* **2008**, *41*, 8095.
(25) Hiltner, A.; Liu, R. Y. F.; Hu, Y. S.; Baer, E. *J. Polym. Sci., Part B: Polym. Phys.* **2005**, *43*, 1047.
(26) Liu, R. Y. F.; Hu, Y. S.; Hibbs, M. R.; Collard, D. M.; Schiraldi, D. A.; Hiltner, A.; Baer, E. *J. Appl. Polym. Sci.* **2005**, *98*, 1615.
(27) Sharma, V.; Desai, P.; Abhiraman, A. S. *J. Appl. Polym. Sci.* **1997**, *65*, 2603.
(28) Orchard, G. A. J.; Spilby, P.; Ward, I. M. *J. Polym. Sci., Part B: Polym. Phys.* **1990**, *28*, 603.
(29) Lin, J.; Shenogin, S.; Nazarenko, S. *Polymer* **2002**, *43*, 4733.
(30) Litvinov, V. M.; Penning, J. P. *Macromol. Chem. Phys.* **2004**, *205*, 1721.
(31) Aharoni, S. M. *Polym. Adv. Technol.* **1998**, *9*, 169.
(32) Gusev, A. A.; Arizzi, S.; Suter, U. W. *J. Chem. Phys.* **1993**, *99*, 2221.
(33) Gusev, A. A.; Suter, U. W. *J. Chem. Phys.* **1993**, *99*, 2228.
(34) Gusev, A. A.; Müller-Plathe, F.; van Gunsteren, W. F.; Suter, U. W. *Adv. Polym. Sci.* **1994**, *116*, 207.
(35) Hofmann, D.; Fritz, L.; Ulbrich, J.; Schepers, C.; Böhning, M. *Macromol. Theory Simul.* **2000**, *9*, 293.

(36) Fedotov, V. D.; Schneider, H. *Structure and Dynamics of Bulk Polymers by NMR Methods. NMR Basic Principles and Progress*; Diehl, P., Fluck, E., Gunter, H., Kosfeld, R., Seelig, I., Eds.; Springer-Verlag: Berlin, 1989.
(37) McBrierty, V. J.; Packer, K. J. *Nuclear Magnetic Resonance in Solid Polymers*; Cambridge University Press: Cambridge, 1993.
(38) Kenwright, A. M.; Say, B. J. In *NMR Spectroscopy of Polymers*; Ibbett, R. N., Ed.; Blackie Academic Professional: London, 1993; p 231.
(39) Schmidt-Rohr, K.; Spiess, H. W. *Multidimensional Solid-State NMR and Polymers*; Academic Press: London, 1994.
(40) Persyn, O.; Miri, V.; Lefebvre, J.-M.; Depecker, C.; Gors, C.; Stroeks, A. *Polym. Eng. Sci.* **2004**, *44*, 261.
(41) Wunderlich, B. *Macromolecular Physics: Crystal Melting*; Academic Press: New York, 1980; Vol. *3*.
(42) Hirschinger, J.; Miura, H.; English, A. *Macromolecules* **1990**, *23*, 2153, 2169.
(43) Litvinov, V. M.; Soliman, M. *Polymer* **2005**, *46*, 3077.
(44) Buda, A.; Demco, D. E.; Bertmer, M.; Blümich, B.; Litvinov, V. M.; Penning, J. P. *ChemPhysChem* **2004**, *5*, 876.
(45) Hedesiu, C.; Kleppinger, R.; Buda, A.; Demco, D. E.; Blümich, B.; Remerie, K.; Litvinov, V. M. *Polymer* **2007**, *48*, 763.
(46) Wouters, M. E. L.; Litvinov, V. M.; Binsbergen, F. L.; Goossens, J. P. G.; van Duin, M.; Dikland, H. G. *Macromolecules* **2003**, *36*, 1147.
(47) Batzer, H.; Kreibich, U. T. *Polym. Bull.* **1981**, *5*, 585.
(48) Krizan, T. D.; Coburn, J. C.; Blatz, P. S. In *Barrier Polymers and Structures*; Koros, W. J., Ed.; ACS Symposium Series 423; American Chemical Society: Washington, DC, 1990; p 111.
(49) Lagaron, J. M.; Gimenez, E.; Catala, R.; Gavara, R. *Macromol. Chem. Phys.* **2003**, *204*, 704.
(50) Hu, Y. S.; Mehta, S.; Schiraldi, D. A.; Hiltner, A.; Baer, E. *J. Polym. Sci., Part B: Polym. Phys.* **2005**, *43*, 1365.
(51) Gavara, R.; Hernandez, R. J. *J. Polym. Sci., Part B: Polym. Phys.* **1994**, *32*, 2375.
(52) Persyn, O.; Miri, V.; Lefebvre, J.-M.; Ferreiro, V.; Brink, T.; Stroeks, A. *J. Polym. Sci., Part B: J. Polym. Phys.* **2006**, *44*, 1690.
(53) Ellis, T. S. *Macromolecules* **1989**, *22*, 742.
(54) Ellis, T. S. *Macromolecules* **1991**, *24*, 3845.
(55) Aerdts, A. M.; Eersels, K. L. L.; Groeninckx, G. *Macromolecules* **1996**, *29*, 1041.
(56) Nishi, T.; Wang, T. T. *Macromolecules* **1975**, *8*, 909.
(57) Ito, M.; Takahashi, A.; Araki, N.; Kanamoto, T. *Polymer* **2001**, *42*, 241.
(58) Miri, V.; Persyn, O.; Lefebvre, J. M.; Sequela, R.; Stroeks, A. *Polymer* **2007**, *48*, 5080.
(59) Gronski, W.; Stadler, R.; Jacobi, M. M. *Macromolecules* **1984**, *17*, 741.
(60) Cohen-Addad, J. P.; Huchot, P. *Macromolecules* **1991**, *24*, 6591.
(61) Brereton, M. G. *Macromolecules* **1993**, *26*, 1152.
(62) Sotta, P.; Higgs, P. G.; Depner, M.; Deloche, B. *Macromolecules* **1995**, *28*, 7208.
(63) Litvinov, V. M. *Macromolecules* **2001**, *34*, 8468.
(64) Sotta, P.; Deloche, B. *Macromolecules* **1990**, *23*, 1999.
(65) Sotta, P. *Macromolecules* **1998**, *31*, 8417.
(66) Cory, D. G.; Ritchey, W. M. *Macromolecules* **1989**, *22*, 1611.
(67) Hirschinger, J.; Hervé, M. *Solid State Nucl. Magn. Reson.* **1994**, *3*, 121.
(68) Hillebrand, L.; Schmidt, A.; Bolz, A.; Hess, M.; Veeman, V. S.; Meier, R. J.; van der Velden, G. *Macromolecules* **1998**, *31*, 5010.
(69) Litvinov, V. M.; Mathot, V. B. F. *Solid State Nucl. Magn. Reson.* **2002**, *22*, 218.
(70) Weeding, T. L.; Veeman, W. S.; Angad Gaur, H.; Huysmans, W. G. B. *Macromolecules* **1988**, *21*, 2028.
(71) Schreiber, R.; Veeman, W. S.; Gabriëlse, W.; Arnauts, J. *Macromolecules* **1999**, *32*, 4647.
(72) Ferreiro, V.; Coulon, G. *J. Polym. Sci., Part B: Polym. Phys.* **2004**, *42*, 687.
(73) Miri, V.; Persyn, O.; Lefebvre, J.-M.; Seguela, R. *Eur. Polym. J.* **2009**, *45*, 757.
(74) Dencheva, N.; Nunes, T.; Oliveira, M. J.; Denchev, Z. *Polymer* **2005**, *46*, 887.
(75) Galeski, A.; Cohen, R. E. *Macromol. Chem.* **1986**, *188*, 1195.
(76) Litvinov, V. M., unpublished results.
(77) Hernandez, R. J. *J. Food Eng.* **1994**, *22*, 495.
(78) Sekelin, D. J.; Stepanov, E. V.; Nazarenko, S.; Schiraldi, D.; Hiltner, A.; Baer, E. *J. Polym. Sci., Part B: Polym. Phys.* **1999**, *37*, 847.
(79) Capitani, D.; Segre, A. L.; Grassi, A.; Sykora, S. *Macromolecules* **1991**, *24*, 623.
(80) Capitani, D.; De Rosa, S.; Ferrando, A.; Grassi, A.; Segre, A. L. *Macromolecules* **1992**, *25*, 3874.
(81) Avakian, P.; Matheson, R. R., Jr.; Starkweather, H. W., Jr. *Macromolecules* **1991**, *24*, 4698.
(82) Khanna, Y. P. *Macromolecules* **1992**, *25*, 3298.
(83) Wunderlich, B. *J. Therm. Anal. Calorim.* **2008**, *93*, 7.
(84) Fukushima, E.; Uehling, E. A. *Phys. Rev.* **1968**, *173*, 366.
(85) Kimmich, R.; Peters, A.; Spohn, K.-H. *J. Membr. Sci.* **1981**, *9*, 313.
(86) Helm, L. *Prog. Nucl. Magn. Reson. Spectrosc.* **2006**, *49*, 45.
(87) Schuster, J.; Cichos, F.; von Borczyskowski, Ch. *Eur. Phys. J.* **2003**, *E12*, S75.
(88) Soong, R.; MacDonald, P. M. *Biophys. J.* **2005**, *88*, 255.
(89) Furó, I.; Dvinskikh, S. V. *Magn. Reson. Chem.* **2002**, *40*, S3 and references therein.
(90) Golodnitsky, D.; Livshits, E.; Ulus, A.; Barkay, Z.; Lapides, I.; Peled, E.; Chung, S. H.; Greenbaum, S. *J. Phys. Chem. A* **2001**, *105*, 10098.
(91) Ferreiro, V.; Pennec, Y.; Séguéla, R.; Coulon, G. *Polymer* **2000**, *41*, 1561.
(92) Ferreiro, V.; Depecker, C.; Laureyns, J.; Coulon, G. *Polymer* **2004**, *45*, 6013.
(93) Taraiya, A. K.; Orchard, G. A. J.; Ward, I. M. *J. Polym. Sci., Part B: Polym. Phys.* **1993**, *31*, 641.
(94) Krishna Pant, P. V.; Boyd, R. H. *Macromolecules* **1993**, *26*, 679.
(95) Capitani, D.; Segre, A. L.; Blicharski, J. S. *Macromolecules* **1995**, *28*, 1121.
(96) Granucci, G.; Persico, M. *Chem. Phys. Lett.* **1993**, *205*, 331.
(97) Gooding, E. A.; Serak, K. R.; Ogilby, P. R. *J. Phys. Chem.* **1991**, *24*, 623.
(98) Pochan, J. M.; Hinman, D. F. *J. Polym. Sci., Polym. Phys. Ed.* **1976**, *14*, 1871.
(99) Kristiansen, M.; Scurlock, R. D.; Iu, K.-K.; Ogilby, P. R. *J. Phys. Chem.* **1991**, *95*, 5190.
(100) Casero, J. J.; Joens, J. A. *J. Phys. Chem. A* **1997**, *101*, 2607.
(101) Casero, J. J.; Joens, J. A. *J. Phys. Chem. A* **1999**, *103*, 7136.
(102) Froix, M. F.; Goedde, A. O. *Polymer* **1976**, *17*, 758.
(103) Dwek, R. A. In *Nuclear Magnetic Resonance in Biochemistry: Applications to Enzym Systems*; Harrington, W., Peacocke, A. R., Eds.; Clarendon Press: Oxford, 1973.
(104) Belmajdoub, A.; Boubel, J. C.; Canet, D. *J. Phys. Chem.* **1989**, *93*, 4844.
(105) Kriwacki, R. W.; Hill, R. B.; Flanagan, J. M.; Caradonna, J. P.; Prestegards, J. H. *J. Am. Chem. Soc.* **1993**, *115*, 8907.
(106) Chien, W.-J.; Cheng, S.-F.; Chang, D.-K. *Anal. Biochem.* **1998**, *264*, 211.